Marine Chemistry 279 (2026) 104696



Contents lists available at ScienceDirect

Marine Chemistry

journal homepage: www.elsevier.com/locate/marchem

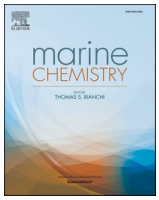

Reactive dissolved nickel distribution in the Northwest Brazilian Continental Shelf: high versus low river discharge periods and the specific role of mangrove forests☆

Cristian H. Krause [a], Nico Fröhberg [b], Leandro M. de Carvalho [a,*], Alexandre B. Schneider [c], Kasley Barreto [a], Andrea Koschinsky [b]

[a] Departamento de Química, Universidade Federal de Santa Maria, C.P. 5051, 97105-970 Santa Maria, RS, Brazil
[b] Department of Physics and Earth Sciences, School of Science, Constructor University, Bremen, Germany
[c] Instituto de Química, Universidade Federal do Rio Grande do Sul, Av. Bento Gonçalves 9500, C.P. 15003, 91501-970 Porto Alegre, RS, Brazil

ARTICLE INFO

Keywords:
Estuaries
Amazon River
Mangroves
Interannual variability
Onboard ship determination

ABSTRACT

The Amazon and Pará river estuaries and the associated plume on the Northwestern Brazilian Continental Shelf constitute a complex and dynamic system that is strongly influenced by seasonal variations in water fluxes. However, few studies have addressed the seasonal and interannual variability of processes that affect the transport of trace metals within this estuarine system. Thus, the goal of this work was to compare the transport of reactive dissolved Ni (dNi) in the Amazon and Pará River estuaries, the associated mixing plume and in the surrounding regions of the Northwest Brazilian Continental Shelf under high- and low-discharge conditions. This study was conducted during *RV Meteor* cruise M206 (GEOTRACES process study GApr21) in the low-discharge period and compared with results from research cruise M147 (GApr11) in the same study area during high-discharge period. Also, surface and porewater samples from a sampling campaign in the mangrove forests in northern Brazil were analyzed. Adsorptive cathodic stripping voltammetry (AdCSV) measurements were carried out onboard immediately after sample filtration (<0.2 μm) and acidification, to quantify the electrochemically active form of the analyte. Surface water samples along the estuary showed similar reactive dNi levels during both high- and low-discharge periods (0.7–9.2 and 0.5–12.6 nmol L^{-1}, respectively), although the salinity gradient was different, mainly due to reduced freshwater influx. Concentrations decreased along the estuary with a non-conservative distribution, indicating that reactive dNi is probably influenced by a combination of input and removal mechanisms. Depth profiles from the continental shelf during both high- and low-discharge periods presented partial depletion of reactive dNi in surface waters and regeneration with depth, likely under the influence of water masses and biogeochemical processes in the water column, consistent with its well-known nutrient-like behavior. No significant concentration differences were observed along the Mangrove belt (1.3–3.7 and 1.4–4.3 nmol L^{-1} during high- and low-discharge periods, respectively), suggesting that reactive dNi in groundwater discharge from Amazonian mangroves is not strongly affected by wet and dry conditions. The reactive dNi trends in the mangrove forests campaign indicate that the enrichment found in mangrove porewaters (65.0–119.5 nmol L^{-1}) represents a local signature, with concentrations decreasing towards the coast due to dilution with seawater. These findings highlight the complex interplay of estuarine mixing, biological cycling, and mangrove-derived inputs in regulating reactive nickel, and demonstrate that river discharge alone is insufficient to predict its transfer from major tropical river systems to the coastal ocean.

1. Introduction

The Amazon and Pará River estuaries, the river plume and the surrounding regions of the Northwest Brazilian Continental Shelf, including the mangrove forests in northern Brazil, are important interfaces for the input of trace metals and dissolved organic matter

☆ This article is part of a Special issue entitled: 'IEBS26 Challenges & Gaps' published in Marine Chemistry.

* Corresponding author.
E-mail address: lemacarvalho@gmail.com (L.M. de Carvalho).

https://doi.org/10.1016/j.marchem.2026.104696
Received 17 July 2026; Received in revised form 12 November 2026; Accepted 13 November 2026
Available online 19 November 2026
0304-4203/© 2026 The Authors. Published by Elsevier B.V. This is an open access article under the CC BY license (http://creativecommons.org/licenses/by/4.0/).
The Article Processing Charge for the publication of this research was funded by the Coordenação de Aperfeiçoamento de Pessoal de Nível Superior - Brasil (CAPES) (ROR identifier: 00x0ma614).

(DOM) into the Atlantic Ocean. The Amazon River discharges about one fifth of the global riverine input into the oceans (Espinoza Villar et al., 2009), which forms a combined mixing plume with the waters from the Pará River estuary. Also, southeast of this area, coastal waters receive contributions from mangrove forests, which impact the biogeochemical cycles of trace elements and DOM with its groundwater discharge (Dittmar et al., 2006; Hollister et al., 2021). Moreover, the mixing zone is influenced by offshore waters from the North Brazil Current (Smoak et al., 2005), thereby connecting inputs from the Amazon and Pará River estuaries and adjacent mangrove forests by transporting the freshwater signal northwest along the Brazilian coast. The freshwater flux to the Atlantic Ocean in this area is strongly affected by seasonal variations. In the Amazon River, the high-discharge period peaks in May–June and the low-discharge period is observed in October–November (Lentz, 1995; Medeiros et al., 2015). Therefore, to estimate yearly elemental fluxes from the river system into the coastal ocean, it is necessary to consider the seasonal and interannual variability of trace metals in this region.

Mangroves grow along about 60–75% of tropical coastlines and act as natural barriers between land and coastal waters (Clough, 1998; McGill, 1958). The mangrove forests of the Amazon region in northern Brazil constitute one of the largest mangrove areas in the world and play an important role in the input of trace metals to the Northwest Brazilian Continental Shelf (Lacerda et al., 2022a). The presence of trace metals in these ecosystems may originate from natural sources, such as rivers, estuaries or tidal waters, or result from anthropogenic pressure, including industrial and mining effluents, sewage discharge or agricultural runoff (Bayen, 2012; Bodin et al., 2013; Yan et al., 2017). Mangrove sediments function as natural sinks for continental materials (Harbison, 1986; Zhang et al., 2014), including trace metals, due to anaerobic and reductive properties and an ecosystem rich in sulfide, organic matter and iron (Silva et al., 1990; Tam, 2006). The fraction in which elements are found in sediments and porewaters provide valuable insights into understanding the biogeochemical cycles and physicochemical speciation of trace elements. Thus, in this study, reactive dNi in mangrove systems - including mangrove porewaters and surface waters from the Caeté River estuary and surrounding creeks - was determined by adsorptive cathodic stripping voltammetry (AdCSV) to evaluate the transport of Ni to the coastal ocean.

AdCSV is an electroanalytical technique capable of detecting low concentrations of trace metals (including speciation analysis, i.e. redox species and organic complexation of environmentally relevant elements) in natural waters (Han and Pan, 2021; Mota et al., 2012) with high sensitivity and selectivity, combining features such as low cost, rapid analysis, and robustness. Moreover, voltametric measurements can be performed with little interference from saline media (Monticelli and Caprara, 2015) and/or DOM. Another advantage of voltammetry is the possibility to be applied onboard, making possible measurements immediately after sampling to minimize the risk of speciation changes during sample storage.

In this study, reactive dNi is defined as the fraction of total dissolved Ni(II) that is electrochemically active and directly measured by AdCSV in acidified samples but without UV digestion of the organic matter, either as a free hydrated ion or an electroactive organic complex (Sander and Koschinsky, 2000). In natural waters, Ni(II) can be present as free ions, bound to organic ligands or inorganic complexes. Additionally, Ni (II) can be adsorpbed onto and incorporated into larger particles formed via the flocculation of inorganic or organic colloids (Motekaitis and Martell, 1987; Byrne et al., 1988). The voltammetric determination of reactive dNi is based on the well-known adsorption/reduction mechanism of the complex *Ni*-dimethylglyoxime (Ni-$(DMG)_2$) on the surface of the mercury electrode (Ma et al., 1997; Baxter et al., 1998). Because of the relative high stability constant of Ni-$(DMG)_2$, Ni(II) can be partially released from weak complexes with DOM in natural waters. Therefore, the proportion of Ni(II) released is a function of the conditional stability constants (log *K*) of the natural organic ligands. Our previous work presents an in-depth discussion about the stripping voltammetric analysis of Ni and Co in natural waters based on DMG complexes. (de Carvalho et al., 2021).

In marine systems, trace metals can occur in different forms, depending on the lability and size fractionation: particulate (>0.2 μm), reactive dissolved and total dissolved (<0.2 μm), large colloidal phase (between 0.2 and 0.015 μm), soluble (between 0.015 μm and 10 kDa), and truly dissolved fractions (< 10 kDa), presenting distinct chemical and physical properties, which affect their mobility, bioavailability and toxicity (Gao et al., 2019; Han and Pan, 2021). Among these metals, Ni participates in various biogeochemical processes: nitrogen fixation, nitrogen uptake, carbon fixation and methanogenesis (Archer et al., 2020; John et al., 2022). Therefore, the knowledge of the physicochemical speciation of Ni helps to understand the biogeochemical cycling, input and removal process that impact the transport of Ni and its interaction with DOM and particulate matter (de Carvalho et al., 2021).

The transport of Ni to the ocean has been extensively studied in estuaries around the world. However, few studies have been reported for the Amazon estuary. In June 1974 and 1976, dissolved Ni concentration ranged to a maximum of 6.9 and 6.3 nmol kg^{-1}, respectively (Boyle et al., 1982). More recently, in April–May 2018, our group found a maximum of 9.2 nmol L^{-1} of reactive dissolved Ni (de Carvalho et al., 2021). These values were similar to the total dissolved concentration, which means the measured fraction corresponds to weakly bound organic Ni complexes that are labile and can exchange Ni with the added competing ligand (DMG) (de Carvalho et al., 2021) or were otherwise easily dissociated from organic ligands after acidification to pH 1.8 (Milne et al., 2010). In addition, other speciation studies have found a higher predominance of labile dissolved Ni compared to non-labile complexes along salinity gradients (Gaulier et al., 2021; Nimmo et al., 1989).

In the study of metals in marine systems, AdCSV is a powerful analytical tool for the speciation analysis of metals, because it can detect different fractions of electrochemical active species (Achterberg and Braungardt, 1999). By applying this method, the aim of the paper was to evaluate the interannual variability of reactive dNi in the Amazon and Pará River estuaries and assess the role of mangrove systems for Ni fluxes into the coastal Atlantic Ocean. Samples were collected in northern Brazil during the low-discharge period in December 2024 (GEOTRACES process study GApr21), including mangrove areas, the Amazon and Pará River estuaries, the associated plume, and surrounding coastal waters. The results were compared with data obtained during the high-discharge period in April/May 2018 (GEOTRACES process study GApr11) in the same study area.

2. Materials and methods

2.1. Sampling and sample treatment: mangrove campaign

The mangrove forest sampling occurred in Mid-November 2024 during a pronounced dry season in northern Brazil (Fig. 1A). The Caeté River estuary is located approximately 200 km southeast of the Pará River estuary. Surface water samples from the Caeté River and the creeks flowing into the river in the mangrove forest were collected from bridges using acid-cleaned buckets, covering sites from locations close to the source of the Caeté River (upstream) to the coastal zone. The sampling of the tributary creeks was repeated during high and low tide downstream of the city of Bragança, the salinity gradient was sampled through the estuary from boats by drawing the surface water with a portable peristaltic pump using Tygon tubing.

The mangrove area was divided by a road built across the vegetation. On one side of the road, the mangrove forest was degraded, with vegetation loss and signs of erosion. In this area, seawater entering during high tide had limited drainage due to the presence of the road. On the other side, the mangrove forest was healthy, with dense vegetation and preserved sediments. On both sides, vegetation was affected by

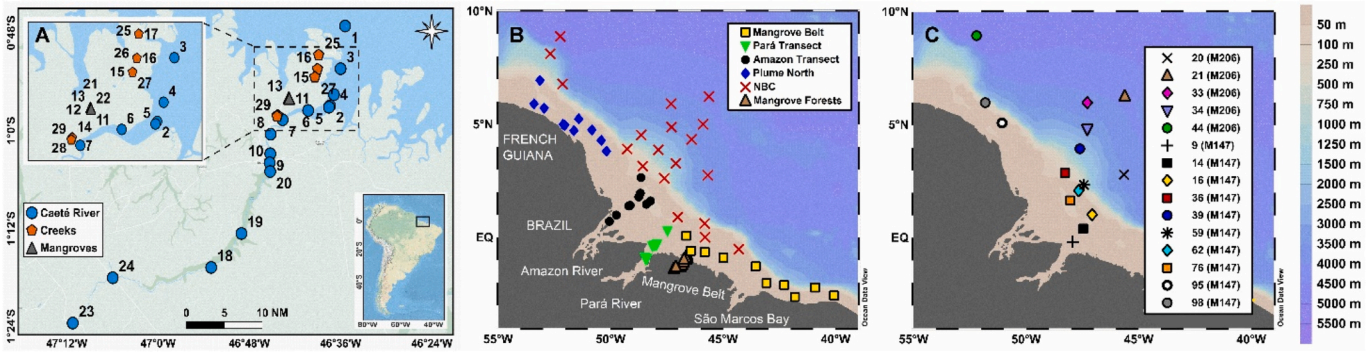

Fig. 1. **(A)** Sampling sites of the mangrove forest campaign across the Caeté River estuary, creeks and mangroves, **(B)** Sampling stations of Amazon and Pará River estuaries, mixing plume and nearby regions of the Northwest Brazilian Continental Shelf obtained during the low-discharge period (M206/mangrove forests campaign) and **(C)** TMR stations with depth profiles from both high- and low-discharge periods. (North Brazil Current, NBC). *QGIS.org (2025), Schlitzer, R., Ocean Data View, https://odv.awi.de, 2025.*

severe drought conditions during the time of sampling. Porewater samples from the sediments of the mangrove forests in the healthy and degraded areas were collected by digging holes to below the water table at low tide that were repeatedly emptied and allowed to refill before sampling until the collected water appeared relatively clear. The porewater samples were then also drawn up by the peristaltic pump, which was used to immediately filter all water samples through polycarbonate filter membranes (0.2 μm pore size, Nuclepore, Whatman, 90 or 142 mm) in metal-free in-line filter holders directly into acid-cleaned low-density polyethylene (LDPE) bottles.

The samples were stored at 4 °C for the duration of the field campaign and acidified to pH < 1.8 with 34% HCl (ROTIPURAN, Carl Roth; final concentration of 0.024 mol L^{-1}) in the beginning of research cruise M206, between 5 and 16 days from sample collection. After acidification, the samples were stored at room temperature for approximately 7 days until analysis.

The samples were numerically classified (1–29), and their origin, including latitude, longitude, salinity, and sample type, are presented in Table 1.

Table 1
Samples characteristics and sources for the sampling campaign in the mangrove region.

Sample	Latitute	Longitude	Salinity	Type of sample
1	−0.79	−46.59	35.0	Caeté River - boat
2	−0.95	−46.62	32.0	Caeté River - boat
3	−0.87	−46.60	34.2	Caeté River - boat
4	−0.93	−46.61	35.2	Caeté River - boat
5	−0.95	−46.62	29.7	Caeté River - boat
6	−0.96	−46.67	27.8	Caeté River - boat
7	−0.98	−46.73	23.1	Caeté River - boat
8	−1.01	−46.75	19.6	Caeté River - boat
9	−1.05	−46.75	15.6	Caeté River - boat
10	−1.07	−46.75	11.7	Caeté River - boat
11	−0.93	−46.71	33.4	Mangroves - degraded area
12	−0.93	−46.71	64.9	Mangroves - degraded area
13	−0.93	−46.71	64.9	Mangroves - degraded area
14	−0.97	−46.73	27.1	Furo do Taici (creek 1)
15	−0.89	−46.65	35.9	Furo da Ostra (creek 2)
16	−0.87	−46.65	34.6	Furo do Meio (creek 3)
17	−0.85	−46.65	33.6	Furo do cafe (creek 4)
18	−1.28	−46.88	0.031	Caeté River - sampling from land
19	−1.21	−46.82	0.019	Caeté River - sampling from land
20	−1.08	−46.75	3.4	Caeté River - sampling from land
21	−0.93	−46.71	42.0	Mangroves - intact area
22	−0.93	−46.71	40.5	Mangroves - intact area
23	−1.39	−47.19	0.023	Caeté River - closest to source
24	−1.30	−47.10	0.018	Caeté River - near source
25	−0.85	−46.65	33.4	Furo do cafe (creek 4)
26	−0.87	−46.65	33.4	Furo do Meio (creek 3)
27	−0.89	−46.66	32.4	Furo da Ostra (creek 2)
28	−0.97	−46.74	21.5	Furo do Taici (creek 1)
29	−0.97	−46.74	26.6	Mangrove well near creek 1

2.2. Sampling and sample treatment: M206 cruise

The GEOTRACES process study cruise M206 (Amazon – GEOTRACES 2, GApr21) took place in December 2024 during the low-discharge period. The sampling procedures for the determination of trace elements were conducted according to the GEOTRACES cookbook (Aguilar-Islas et al., 2024).

The surface water samples were collected with a tow-fish pump sampler in the Amazon and Pará river estuaries and associated mixing region and in the coastal water around the Mangrove Belt. During the sampling procedure (while the ship was steaming), the tow-fish (a torpedo-shaped pump unit) submerged into the water at ~2 m water depth while being towed by a starboard crane from the stern of the research vessel. Water samples from the tow-fish were pumped into the trace element clean bubble using a Teflon-diaphragm pump and acid-washed braided polyvinyl chloride (PVC) tube.

The water column samples were collected at different depths (~10 to 4000 m) with a trace metal clean rosette water sampler (TMR). Trace metal clean GO-FLO-type samplers was constructed from a titanium frame with an autonomous control unit (1018 intelligent, General Oceanics) with up to 12 metal free samplers (5 L Model 114, OceanTestEquipment & 8 L GO-FLO, General Oceanics were both used during this cruise). The TMR was deployed with the vessel's polyethylene-jacketed aramid rope winch to avoid contamination from steel cables. Sample depths were pre-programmed before deployment and automatically triggered using the integrated pressure sensor of the system. After recovery, the TMR bottles were immediately carried to the trace element clean bubble which was equipped with an air-filtration unit to create near-clean-room conditions for sample processing.

The tow-fish samples as well as the TMR samples were filtered through 0.8/0.2 μm cartridge filters (AcroPak™) into 100 mL acid washed polyethylene terephthalate (PET) bottles and acidified to pH < 1.8 with 34% HCl (ROTIPURAN, Carl Roth; final concentration of 0.024 mol L^{-1}) to obtain the dissolved fraction. The samples were then transferred to the voltammetry laboratory and kept at room temperature until onboard AdCSV measurements were carried out (Koschinsky et al., 2025), usually on the same day or the following day.

The samples collected during the *RV Meteor* M206 were classified for analysis according to the salinity and source into the following groups: Mangrove Belt, Pará Transect, Amazon Transect, Plume North and North Brazil Current (NBC) (Fig. 1B). The first set of samples was collected in the Mangrove Belt. This region was parallel to mangrove forests and showed high salinities between 36.0 and 37.0. The Pará River transect, with the freshwater sources being the Tocantins River in the south, the

main Pará River and other narrower channels and creeks, consisted of samples with salinities between 2.7 for the river near Belém, and 36.0 on the seawater side. In the Amazon River outflow area, the Amazon River transect showed salinities between 0.030 for the river end member and around 36.0 for the seawater end member. To the north, the Plume North transect involved stations with salinities higher than 35.0. Also, the offshore stations were under the influence of the NBC, which flows along the coast of Northern Brazil, with salinities around 36.0. Conductivity was measured immediately upon the sample's arrival on board using the YSI EcoSense EC300A Conductivity/Temperature meter, and the values were converted to salinity. Depth profile stations from both high-and low-discharge periods are shown in Fig. 1C.

2.3. Sample mixing experiments

Due to the extremely dry season preceding our cruise M206, the river plume was confined to the river mouth and did not produce a smooth mixing gradient with seawater. Instead, there was a sudden change in salinity across the Amazon Transect, ranging from low values in the river mouth ($S \leq 1.0$) to ca. 16 almost immediately within a distance of about 4 nautical miles. Therefore, to obtain a better resolution with a larger number of samples at different salinities on the Amazon Transect, sample mixing experiments were conducted onboard. The sample mixing was performed as follows: an Amazon River end member sample (reactive dNi = 4.7 nmol L^{-1}, S = 0.030) was mixed with a seawater end member sample (reactive dNi = 2.5 nmol L^{-1}, S = 36.5) in different proportions resulting in salinities of 1.8, 2.6, 4.0, 8.0, 12.0, 16.0, 20.0 and 25.0. The samples were added to Cubitainers (collapsible polyethylene containers) previously washed with 1.0 mol L^{-1} HCl and ultrapure water, shaken and allowed to equilibrate for a day and then filtered through a 0.2 μm polycarbonate filter (Nuclepore, Whatman). Temperature and pH were measured at the start and at the end of the experiment.

2.4. Reagents and solutions

All chemicals used in the preparation of working solutions were of analytical ultrapure reagent grade. The ultrapure water (18.2 MΩ cm) was obtained from a Milli-Q® system (Millipore, Bedford, USA). A 170 μmol L^{-1} Ni stock solution was prepared weekly by a suitable dilution of 1000 mg kg^{-1} standard solution of Ni from SpecSol® (Quimlab, Jacareí, Brazil) and sequentially diluted daily to 17.0 μmol L^{-1} and 0.68 μmol L^{-1} using 0.010 mol L^{-1} HCl. The 0.10 mol L^{-1} dimethylglyoxime (DMG) stock solution was prepared by dissolving the respective amount of the solid (Sigma-Aldrich, St. Louis, USA) in ethanol (95%, *v*/v). A 2.0 mol L^{-1} ammonium buffer (pH 9.5) was prepared by mixing and dilution of the proper amount of 20% ammonia solution (ROTIPURAN, Carl Roth) with 34% HCl.

2.5. Apparatus

Differential pulse voltammograms were recorded onboard using an Autolab PGSTAT302N potentiostat combined with a 663 VA Stand through an IME663 interface and the software NOVA® version 2.1.7 was used for data acquisition (Metrohm, Herisau, Switzerland). The voltametric measurements were carried out in a conventional 5–70 mL borosilicate voltametric cell, including a Multi-Mode Electrode (MME) in hanging mercury drop electrode (HMDE) mode as working electrode, a platinum (Pt) rod electrode (2 mm diameter) as auxiliary electrode and all potentials were measured against an Ag/AgCl/KCl (3.0 mol L^{-1}) reference electrode (all from Metrohm). For the pH measurements, a pH meter (Akso, São Leopoldo, Brazil) was used, which was calibrated daily. Before use, the voltammetric cells and plastic materials were left for 48 h in a solution containing 10% HNO_3 (*v*/v), followed by thorough rinsing with ultrapure water.

2.6. Analytical procedure

The onboard AdCSV determination of reactive dNi was carried out in 0.2 μm filtered and acidified samples. The voltammetric measurements were performed in a cell containing 10.00 mL of sample, 500 μL of 2.0 mol L^{-1} ammonium buffer (final pH = 9.0 ± 0.2) and 50 μL of 0.10 mol L^{-1} DMG (concentration in the cell: 0.47 mmol L^{-1}). Then, the solution was de-aerated with nitrogen gas (N_2, 5 N, Air Liquide) for 5 min. An adsorption potential (E_{ads}) of −0.60 V was set for 15 s adsorption time (t_{ads}) under stirring at 1.500 rpm, followed by a 15 s equilibration time. Afterwards, the voltammograms were recorded by a cathodic sweep of the potential from −0.60 V to −1.20 V in differential pulse mode with a pulse amplitude (ΔE_{pulse}) of −50 mV, a pulse duration (t_{pulse}) of 40 ms and a scan rate (SR) of 10 mV s^{-1}. Standard addition calibration curves were acquired by adding 50 or 100 μL of the 0.68 μmol L^{-1} Ni working solution three times in the voltametric cell (resulting in 3.3, 6.5 and 9.7 or 6.5, 13.0 and 19.4 nmol L^{-1}, respectively), according to different Ni concentration ranges in the samples. The peak potential for the reduction of Ni-$(DMG)_2$ was −0.95 V. The blanks were measured in a voltammetric cell containing 10.00 mL of ultrapure water instead of sample and the same volumes of ammonium buffer and 0.10 mol L^{-1} DMG as any other sample analysis. The analytical characteristics of the analytical method is presented in the Supplementary Material.

3. Results and discussion

3.1. Distribution of reactive dNi: high vs low river discharge periods

3.1.1. Spatial distribution of reactive dNi

Studies on the investigation of Ni in the Amazon and Pará estuaries, the associated plume and in the Mangrove Belt located southeast of the Pará River outflow area are scarce (Boyle et al., 1982; de Carvalho et al., 2021; Hollister et al., 2022). This work presents, for the first time, a comparative analysis of reactive dNi concentration in the Amazon and Pará Rivers estuaries, the associated plume and in the surrounding areas of the Northwest Brazilian Continental Shelf, during both high- and low-discharge periods. Figs. 2A-B shows the distribution of reactive dNi in different transects obtained during the high-discharge period (M147, empty symbols) and the low-discharge period (M206, colored symbols). Along the Amazon Transect in the low-discharge period, samples with salinities 1.8, 2.6, 4.0, 8.0, 12.0, 16.0, 20.0 and 25.0 were obtained from mixing experiments carried out onboard (Fig. 2B), as described in the section *Sampling and sample treatment*.

Fig. 3A-B illustrates a comparison of the spatial distribution of salinity and reactive dNi in the study area during both high- and low-discharge periods. For comparison purposes, both figures are presented at the same scale.

Similar reactive dNi concentration ranges were observed during both high- and low-discharge periods. However, the salinity gradient was different, due to strongly differing freshwater influx, resulting in seasonal variations in reactive dNi distribution along the estuary. Voltammetric measurements in the samples collected under high-discharge conditions (M147) presented reactive dNi concentration in the range of 0.7 to 9.2 nmol L^{-1}, while in the low-discharge period (M206), concentrations ranged from <0.5 to 12.6 nmol L^{-1} (Fig. 3A-B). During both cruises, higher concentrations of reactive dNi were observed in the Pará River estuary compared to the Amazon River estuary, indicating distinct influences from the Amazon and Pará rivers as natural sources of Ni. The samples with the lowest salinity in the Pará River (S = 2.7 and 3.6) during the low-discharge period (M206) contained 5.6 and 12.6 nmol L^{-1} of Ni, respectively, while the Pará River end member in the high-discharge period (M147) was 9.2 nmol L^{-1} at S = 0.35. The Amazon River end member samples (4.7 nmol L^{-1}, S = 0.030 and 6.9 nmol L^{-1}, S = 0.10) in the low-discharge period showed very similar Ni concentrations as the ones obtained under high-discharge conditions

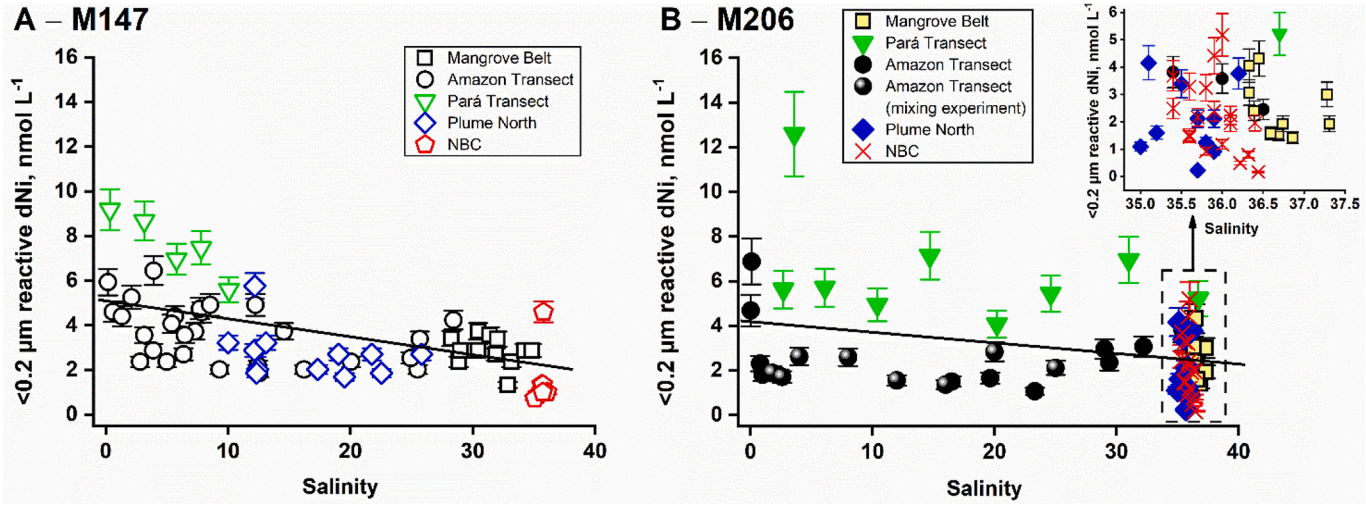

Fig. 2. Comparative distribution of reactive dNi along the salinity gradient in samples collected during **(A)** high-discharge period (M147) according to de Carvalho et al. (2021) and **(B)** low-discharge period (M206). The sampling stations were categorized according to their location on both expeditions. For the mixing experiments, an Amazon River end member sample (4.7 nmol L^{-1}, S = 0.030) was mixed with a seawater end member sample (2.5 nmol L^{-1}, S = 36.5).

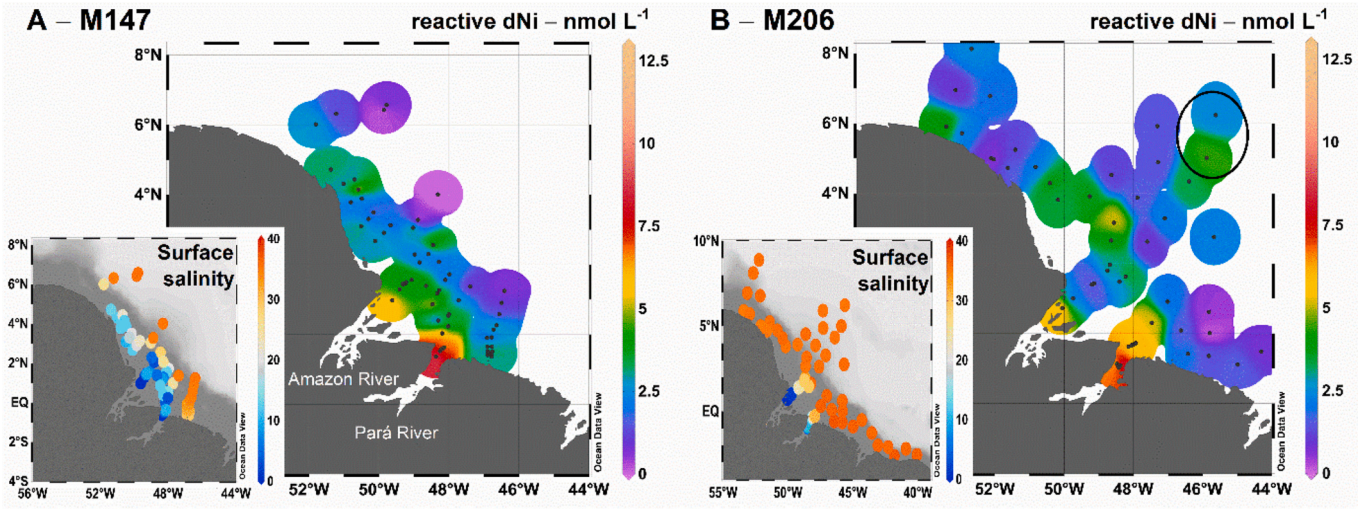

Fig. 3. Spatial distribution of reactive dNi and surface salinity in the study area in the **(A)** high-discharge period (M147) and **(B)** low-discharge period (M206), the circle highlights increased Ni concentrations which are likely related to the circumflexed part of the Amazon plume during the dry season (see text). *Schlitzer, R., Ocean Data View, https://odv.awi.de, 2025;* graphic A was adapted from de Carvalho et al. (2021).

(5.9 nmol L^{-1}, S = 0.18). Additionally, statistical analyses were performed to evaluate differences in Ni concentrations between the M147 and M206 sampling campaigns. Data normality was assessed using the Shapiro–Wilk test. Because the normalized data were not normally distributed, a two-tailed Mann–Whitney *U* test was used to compare the two independent campaigns. The test indicated no statistically significant difference in Ni concentrations between the two distributions ($p = 0.1728$).

Reactive dNi concentrations decreased with increasing salinity during both high- and low-discharge periods. Previous studies on Ni speciation in estuaries also reported a decrease in dissolved Ni concentration along the salinity gradient (Boyle et al., 1982; Martino et al., 2004; Turner et al., 1998; van den Berg et al., 1991). Salinity data indicated a restriction of the freshwater plume to the river mouth of the Amazon and Pará rivers during the low-discharge period (M206). In contrast, in the high-discharge period (M147), the waters of the Amazon and Pará river estuaries mixed to form a plume at intermediate salinities (S = 10.0–25.0) that converged to the north (de Carvalho et al., 2021), as can be seen in Fig. 4A-B.

3.1.2. *Reactive dNi in the Amazon and Pará estuaries*

The Amazon and Pará rivers exhibit pronounced seasonal and interannual variability in discharge and water level, which strongly influences the delivery of dissolved and particulate material to the estuary. At the Óbidos gauging station, representing most of the Amazon Basin discharge, the river typically reaches high-water conditions between April and June and low-water conditions between October and December (Prestes et al., 2020). In 2018, annual mean discharge at Óbidos was about 180,000 $m^3\ s^{-1}$, with May corresponding to the rising/high-water phase; our May 2018 cruise therefore sampled the Amazon–Pará estuary during a period of comparatively high freshwater discharge. In contrast, December 2024 occurred during an exceptional low-water period following the severe Amazon drought of 2023–2024, when annual discharge at Óbidos was substantially lower than in 2018 (about 199,000 $m^3\ s^{-1}$ in 2024 versus 180,000 $m^3\ s^{-1}$ in 2018 according to annual statistics, although the annual means obscure the strong seasonal contrast (source: SO-HYBAM Amazon Water Basin Resources Observation Service online http://www.ore-hybam.org). The Pará River has a distinct seasonal regime, with discharge peaking around

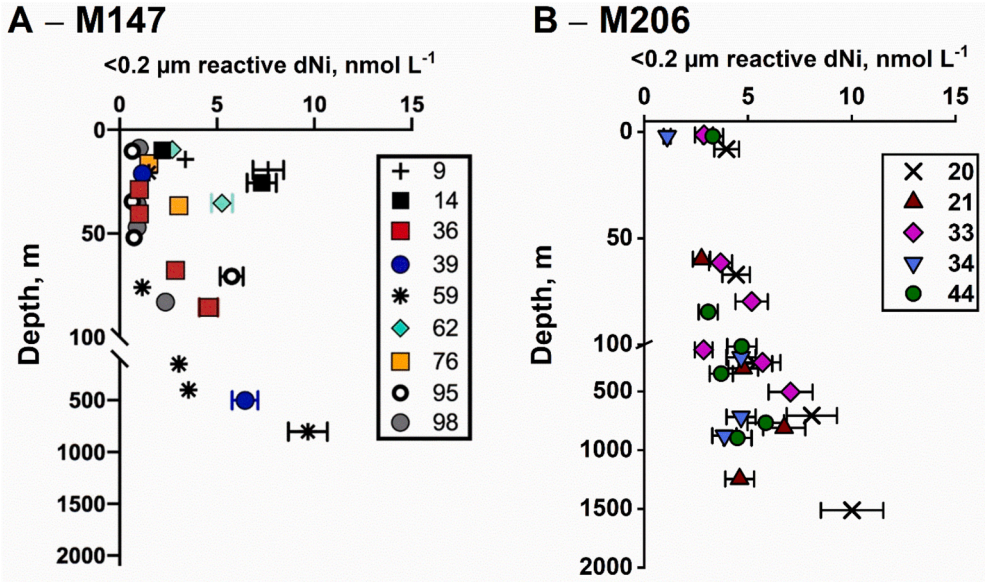

Fig. 4. Comparison of depth profiles of reactive dNi (<0.2 µm) measured in samples collected from TMR bottles during **(A)** high-discharge period (M147) and **(B)** low-discharge period (M206) in the study area, graphic A was adapted from de Carvalho et al. (2021).

April–May and reaching minimum values in October–December; its long-term mean discharge is approximately 21,000 m^3 s^{-1}. Thus, the May 2018 and December 2024 cruises captured contrasting hydrological states of the Amazon–Pará system, providing an opportunity to assess how strongly seasonal and drought-related changes in freshwater input influence trace-metal transport and estuarine processing.

During the high-discharge period (M147), reactive dNi concentrations decreased with increasing salinity but exhibited non-conservative distribution (Fig. 2A). A mid-salinity local minimum (between 12.4 and 25.5), considering both the Amazon transect and the Plume North, was attributed to biological uptake and/or colloidal flocculation. Indeed, these findings were supported by elevated chlorophyll *a* level in this salinity range (Hollister et al., 2021), and a large fraction of colloidal Ni in low-mid salinity range, indicating colloidal flocculation at higher salinities (de Carvalho et al., 2021). An increase in reactive dNi concentrations was observed following the local minima at intermediate salinities ($S \geq 16.0$), which may be associated with desorption from particles (Morris et al., 1965; Coleman, 1966). However, this increase may also reflect changes in Ni speciation within the <0.2 µm fraction, and therefore does not necessarily indicate an increase in total dNi concentrations. Under low-discharge conditions (M206), considering both the collected samples and those prepared from mixing experiments along the Amazon Transect, a strong removal of reactive dNi was observed at low salinities (between 0.8 and 1.0), likely caused by rapid mixing with seawater, followed by a minimum extending up to salinities of 23.3. As more seawater mixed with river water, a slight increase in reactive dNi concentrations was also observed ($S > 23.3$). As total dNi data are not available due to limited analytical capacities during the cruise, an assessment of the reactive Ni fraction compared to the total concentration and a comparison with total Ni concentrations of the wet season sampling campaign M147 are not possible.

Considering the Pará River outflow area, a minor decrease in reactive dNi concentrations with increasing salinity was observed in the high-discharge period (M147), while during the low-discharge period (M206) no clear evidence of removal at intermediate salinities was detected, with concentrations remaining relatively constant throughout the estuary. Even with distinct salinity gradient profiles under high- and low-discharge conditions in the same area, the elevated reactive dNi background represents a continuous input of Ni to the Northwest Brazilian Continental Shelf. Higher reactive dNi levels in the Pará River outflow area may be linked to different Ni sources in the catchment area. Furthermore, previous studies have demonstrated enrichment of Ni in surface sediments of the Guajará Bay (a shallow estuarine embayment that forms part of the Pará River system near the city of Belém) due to influence of commercial and industrial activities (Costa de Souza et al., 2025). In addition, Ni contamination due to mining activities have been extensively reported in the whole Amazon basin (Melfi et al., 1988; Oliveira et al., 1992; Moulatlet et al., 2023).

3.1.3. *Reactive dNi in the Amazon plume and NBC region*

All the stations in the Plume North transects showed high salinities ($S \geq 35.0$) due to the significantly lower freshwater flux (Fig. 3A-B) compared to the high-discharge period (M147), when salinities ranged from 10.0 to 25.8. During the high-discharge period, this region received waters from both source rivers, which converged to form a plume of intermediate salinity (10.0–26.0) that flowed to the north during the rainy season (de Carvalho et al., 2021). In contrast, under low-discharge conditions (M206), the river plume was confined to the river mouth and did not produce a smooth mixing gradient with seawater; consequently, the results reflected only high salinity waters with slightly lower reactive dNi concentrations compared to the high-discharge period, probably due to the lack of formation of a significant plume by the Amazon and Pará Rivers.

The Amazon and Pará river basins contribute a large volume of freshwater to the Northwest Brazilian Continental Shelf; in addition, this region also receives a substantial amount of seawater in the mixing zone. Indeed, the outer Amazon continental shelf is characterized by highly energetic hydrodynamic conditions, including the influence of the North Brazilian Current and strong tidal forcing (Smoak et al., 2005). The large number of samples with salinities higher than 35.0 across multiple transects (low-discharge period, M206), including those collected in the Mangrove Belt (discussed in Section *The Ni contribution by the Mangrove Belt*), indicates early mixing with seawater and a strong oceanic influence in the coastal region during the pronounced dry season preceding the M206 campaign.

Offshore stations ($S \geq 35.0$) with waters under the influence of the NBC exhibited reactive dNi concentrations between 0.5 and 5.2 nmol L^{-1} (with one station showing a concentration below the LOQ) throughout the low-discharge period (M206). In the high-discharge period (M147), a similar trend was observed for the NBC stations, with a concentration range between 0.7 and 4.6 nmol L^{-1}, showing high variability in this dynamic environment because of the different

freshwater sources, including the Amazon and Pará rivers and mangroves forests to the south. Nevertheless, during the low-discharge period, slightly higher reactive dNi concentrations (2.5–4.4 nmol L^{-1}) were observed at the northeastern end of the sampling track (around 6°N, see circle in Fig. 3B). Furthermore, an increase in chlorophyll concentrations and a decrease in surface water salinity of up to 0.40 towards this region was observed (Koschinsky et al., 2025). The overall picture of the study area (supported by satellite data) shows that the river plume, which moves north-westwards along the coast with the North Brazil Current (NBC), splits into two parts in the border area between French Guyana and Suriname at about 9°N. One part moves further north-west towards the Caribbean and the other changes direction due to the influence of the North Equatorial Counter Current (NECC) and flows back to the south-east where it is held at about 6–8°N by an eddy. The slightly increased chlorophyll concentrations as well as the increased reactive dNi concentrations indicate that there are likely still enough nutrients being transported from the Amazon plume into this region to measurably increase phytoplankton productivity. These observations indicate that, despite the strongly reduced freshwater input during cruise M206 and the intense mixing with seawater, the Amazon plume can still impact the biogeochemistry of surface water in regions far away from the river mouth. The measured Ni concentration likely represents the difference between the original river-sourced Ni concentration at this sampling point and the fraction that was removed from it due to biological uptake.

3.2. Depth profiles

Fig. 4A-B shows the distribution of reactive dNi throughout the water column in samples collected from TMR bottles during both high- and low-discharge periods. At the five depth profile stations studied in the low-discharge period (M206) (Fig. 1C), the concentrations of reactive dNi ranged from 1.1 to 10.0 nmol L^{-1} (1.4–1511 m), which is in the same range obtained in the high-discharge period (M147) (ca. 1–10 nmol L^{-1}). In the upper water column samples collected from TMR bottles ($\leq$ 25 m), reactive dNi ranged from 1.1 to 4.0 nmol L^{-1} throughout the low-discharge period, which was very similar to the surface data obtained from tow-fish stations (ca. 2 m deep, between 1.4 and 3.2 nmol L^{-1}). Similar Ni concentrations for both sampling campaigns indicate that fluvial discharge during different seasons had a limited influence on reactive dNi in surface waters. In addition, lower concentrations relative to deeper waters suggest biological uptake in the photic zone (Archer et al., 2020; John et al., 2024).

Increasing concentration of reactive dNi with water depth confirms a nutrient-like behavior, with remineralization processes playing an important role in controlling Ni concentrations throughout the water column (Sclater et al., 1976; Bruland, 1980; Twining et al., 2012; John et al., 2022).

Under high-discharge conditions (M147), a minimum in reactive dNi concentrations was observed between 30 and 60 m, which can be attributed to removal processes such as biological uptake and/or particle adsorption. This minimum was not observed throughout the low-discharge period (M206), likely due to the absence of sampling within this depth interval. At intermediate depths (50–500 m), reactive dNi concentrations showed greater variability. Indeed, the distribution of Ni in the water column may be influenced by a combination of processes, including particle scavenging, biological uptake and regeneration (Balistrieri and Murray, 1986; Tani et al., 2004; Hollister et al., 2020).

In deeper waters (>500–1000 m), the increase in reactive dNi concentrations likely reflects regeneration processes and/or the influence of Antarctic Intermediate Water (AAIW) masses (Hawco et al., 2018). During the low-discharge period (M206), conductivity–temperature–depth (CTD) observations identified several water masses in the water column, including the Antarctic Intermediate Water, characterized by a salinity minimum, and the North Atlantic Deep Water, with higher salinity, lower temperature, and higher oxygen levels (Koschinsky et al., 2025).

The similarity of the data obtained during both high- and low-discharge periods suggests that inputs from the Amazon and Pará rivers have a limited influence on Ni distribution across the water column. The results of this study indicate a partial depletion of reactive dNi in surface waters and an increase with depth. The combined depth profile data from both high- and low-discharge periods indicate that influence from water masses and biogeochemical processes in the water column play a primary role in the cycling of reactive dNi in this estuarine environment.

The vertical distributions of reactive dNi during both cruises indicate that the influence of river discharge is superimposed on a persistent oceanic water-mass control. During the high-discharge M147 cruise, the shallow profiles show pronounced freshwater stratification and strong biological and particle dynamics, particularly at stations influenced by the Amazon plume. At Station 9, for example, reactive dNi increased from approximately 5–6 nmol L^{-1} near 14 m to 7–8 nmol L^{-1} at ~20 m, coincident with increasing salinity and strong changes in chlorophyll fluorescence and beam attenuation. Similar shallow subsurface increases are evident at Stations 36, 59, 62, 76, 95 and 98. Importantly, the deeper M147 profiles at Stations 59 and 96 show that reactive dNi also increases below the surface layer and reaches elevated concentrations at several hundred meters depth, demonstrating that the subsurface Ni enrichment is not restricted to the low-discharge conditions observed during M206. At M206, reactive dNi likewise generally increases below the productive surface layer, although the depth and magnitude of the enrichment vary among stations. The hydrographic profiles from both cruises indicate the transition from warm, saline Tropical Surface Water through South Atlantic Central Water (SACW) and AAIW, with deeper waters increasingly reflecting North Atlantic Deep Water (NADW). These water masses have distinct temperature–salinity characteristics and biogeochemical histories, and their mixing is known to exert a major control on the distribution of Atlantic Ni (Stramma and England, 1999; Middag et al., 2020). The recurring increase in reactive dNi below the surface layer is consistent with nutrient-type behavior and regeneration following biological uptake, but the differences in the depth and magnitude of the maxima among stations and between cruises indicate that regeneration alone cannot explain the profiles. Instead, the observed distributions likely reflect the combined effects of surface biological cycling, regeneration at depth, and the advection and mixing of water masses with different preformed Ni concentrations. The seasonal river-discharge signal therefore appears to be strongest in the shallow, Amazon-influenced plume, whereas the subsurface and deeper reactive dNi distributions are governed increasingly by biological cycling and regional water-mass structure.

3.3. The Ni contribution by the Mangrove Belt

Results from the high-discharge period (M147) highlighted the importance of the mangrove forests located southeast of the Pará River outflow area for the input of trace metals and DOM into the Northwest Brazilian Continental Shelf. Indeed, slightly elevated levels of Ni, cobalt (Co) and titanium (Ti) in coastal waters off the Amazonian Mangrove Belt were observed and linked to submarine groundwater discharge (de Carvalho et al., 2021; Hollister et al., 2021; Schneider et al., 2022: Xu et al., 2025), which indicates that Amazonian mangroves act as sources of nutrients and trace metals to the coastal ocean (Dittmar et al., 2006; Matos et al., 2022). Because of these results, a larger number of stations were planned in this region for the low-discharge period (M206) (Mangrove Belt transect in Fig. 1B). Samples were collected at 14 stations between Fortaleza and the Rio Pará mouth to assess the influence of the mangrove rivers and groundwater discharges on trace metal fluxes into the coastal Atlantic Ocean. Due to sampling permission limitations, however, getting very close to the coast was not allowed, and a position a few nautical miles away from the coastline had to be maintained.

Reactive dNi concentrations in the Mangrove Belt (1.3–3.7 and

1.4–4.3 nmol L^{-1} obtained in the high- and low- discharge periods, respectively) did not differ significantly (Fig. 3A–B and 6A-B), according to a two-sample Student's *t*-test ($p > 0.05$). These results highlight the role of mangroves in the Amazon region as a source of reactive dNi, regardless of the season.

The transport of nutrients and DOM from mangroves – coastal intertidal systems - to the ocean occurs primarily through groundwater discharge (Dittmar and Lara, 2001). Mangroves in the Amazon region are considered one of the major sources of DOM and nutrients to the Northwestern Brazilian Continental Shelf (Dittmar et al., 2001; Dittmar et al., 2006). Nickel may be exported from Amazonian mangroves associated with particulate matter and dissolved organic complexes. During mixing of groundwater and seawater, desorption of trace metals or dissociation of Ni-DOM complexes may occur, contributing to the reactive dNi observed during both high- and low-discharge periods.

The highest reactive dNi concentrations in the Mangrove Belt during the low-discharge period (M206) was observed at sampling stations near the Bay of São Marcos (Fig. 5A-B, encircled symbols). This area is influenced by the hydrographic basin of the Mearim River. Environmental conditions in this region include harbor activities, deforestation, a decommissioned landfill, industrial and domestic sewage inputs, and rapid urbanization (Santos et al., 2023). Hence, anthropogenic activities may contribute to these high Ni concentrations.

The results for the sampling campaign in the mangrove forests are presented in Fig. 7A-C. From station 23 (Caeté River, closest to the source of the Caeté; Fig. 1A, Table 1) towards the coast, elevated levels of reactive dNi were observed at mid-salinity (10.0–30.0) as the sampling stations approached the mangrove area. This was followed by a decrease in Ni concentrations in samples collected closer to the seawater end member due to dilution with low-Ni seawater.

The lowest reactive dNi concentrations were observed in samples collected at the southernmost stations (18, 19, 23, and 24 in Fig. 1A, all with $S \leq 1.0$). Concentrations at these stations (0.9–2.1 nmol L^{-1}) were lower than those reported for low-salinity samples in the Amazon and Pará rivers in the same low-discharge period (M206) (4.7 nmol L^{-1}, $S = 0.030$ and 6.9 nmol L^{-1}, $S = 0.10$ for the Amazon River and 5.6 nmol L^{-1}, $S = 2.7$ and 12.6 nmol L^{-1}, $S = 3.6$ for the Pará River), indicating that the Caeté River represents a minor source of reactive dNi compared to the Amazon and Pará rivers. The increased reactive dNi concentration observed at station 20 (Caeté River; 11.1 nmol L^{-1} at $S = 3.4$) towards the north occurred as sampling approached the mangrove area, which is mainly attributed to the capacity of mangroves to accumulate trace metals (Harbison, 1986; Zhang et al., 2014), but also to Ni desorption from particles and the formation of Ni chloride complexes.

In the mangrove area, salinities up to twice that of seawater were found in porewater of the degraded area, indicating a dominance of evaporation over freshwater inflow during the extreme drought. Nevertheless, slightly higher reactive dNi concentrations were found in the intact mangrove area at salinity only slightly higher than seawater (Fig. 6B). These reactive dNi levels in mangroves may be related to biogeochemical processes, such as sediment oxidation and altered physicochemical conditions. Indeed, mangroves act as sinks, accumulating trace metals in their sediments. This behavior is controlled by factors such as organic matter content, pH, redox potential (Eh), microbial activity, and anoxic conditions, which favor precipitation of trace metals as sulfides. Mangroves are also exposed to tidal cycles, and potentially to urban impact and/or industrial contamination. The release of trace metals to porewater may occur because of variations in chemical and physical properties, such as changes in Eh, pH, and salinity (Harbison, 1986; Lacerda et al., 1988; Bayen, 2012; Yan et al., 2017; Lacerda et al., 2022b). Most of Ni accumulated in mangrove sediments is bound to the refractory phase (silicates, oxides and stable mineral phases) that are not available for porewater exchange. Consequently, only trace metals associated with iron-manganese oxyhydroxides, dissolved organic matter, and reactive sulfides can potentially be mobilized into porewater (Marchand et al., 2016; Chakraborty et al., 2015) (Marchand et al., 2012). Therefore, the very high reactive dNi concentrations in the mangrove porewaters confirm findings by Xu et al. (2025) that the Amazonian Mangrove Belt supplies trace elements through porewater discharge, dissolution of iron-manganese oxyhydroxides and their interactions with seawater. Lastly, we observed that reactive dNi and total dNi yielded Ni concentrations in the same range (Fig. 6B). The similar trends observed here indicate that the majority of dissolved Ni species are present as relatively labile complexes, as already observed in previous work (de Carvalho et al., 2021).

4. Conclusions

This study provides the first comparison of reactive dissolved Ni (dNi) in the Amazon–Pará estuarine system and adjacent Northwest Brazilian Continental Shelf under contrasting high- and low-discharge

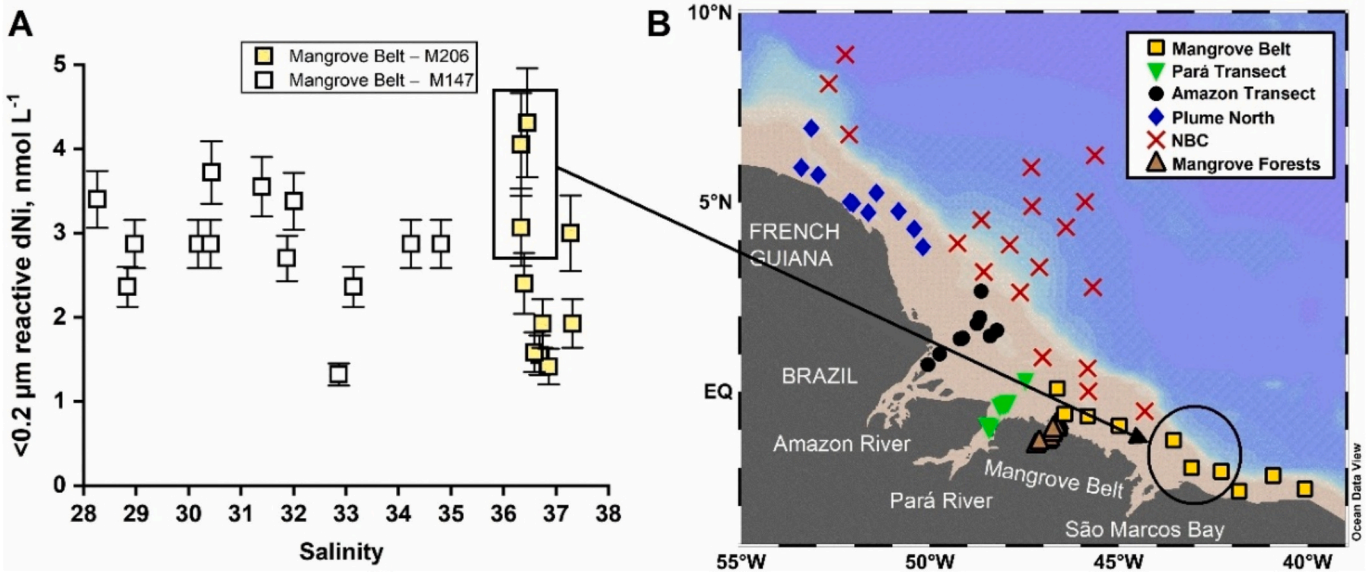

Fig. 5. **(A)** Distribution of reactive dNi across the Mangrove Belt during both high- and low-discharge periods. **(B)** Elevated concentration of reactive dNi found in stations near the Bay of São Marcos (circled symbols). *Schlitzer, R., Ocean Data View, https://odv.awi.de, 2025.*

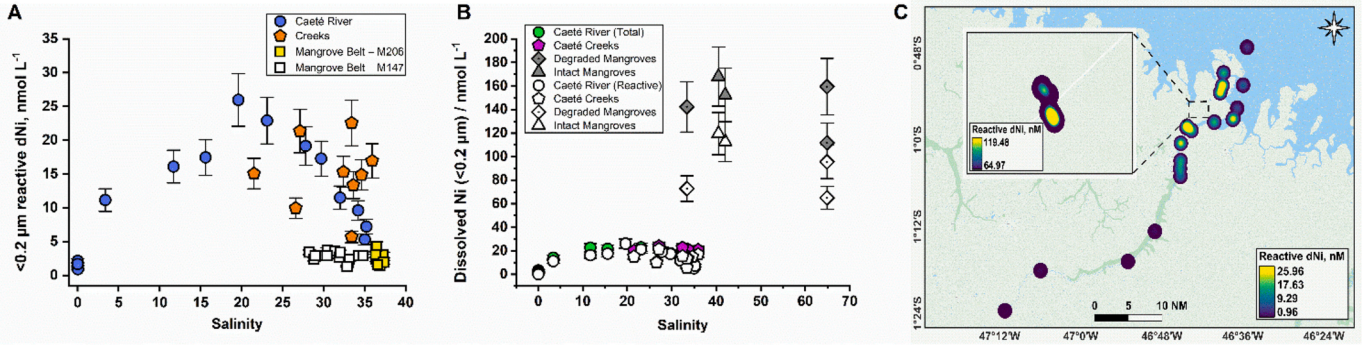

Fig. 6. Comparative distribution of reactive dNi along the salinity gradient during the mangrove forest campaign: **(A)** comparison with Mangrove Belt samples from both the two cruises during high- and low-discharge periods excluding porewater samples; **(B)** comparison including porewater samples; and **(C)** kernel density map of reactive dNi across the sampling sites.

conditions, complemented by measurements in Amazonian mangrove environments. Despite pronounced seasonal differences in river discharge and salinity structure, reactive dNi concentrations in the coastal and shelf waters were broadly similar between the two periods. Within the estuaries dNi showed non-conservative behavior and generally decreased with increasing salinity, indicating that riverine Ni is substantially modified during estuarine mixing through a combination of removal and recycling processes, including colloidal and biological interactions.

The vertical profiles provide further evidence that the seasonal riverine signal is largely restricted to the shallow plume, whereas subsurface and deeper dNi distributions are additionally controlled by biological cycling and oceanic water-mass structure. Under high-discharge conditions, the M147 profiles show pronounced freshwater stratification and strong biological and particle dynamics in the upper tens of metres, accompanied by relatively elevated reactive dNi. At greater depths, however, elevated dNi was also observed during M147, as well as throughout the M206 profiles obtained under low-discharge conditions. The recurring increase of dNi below the productive surface layer is consistent with biological uptake and regeneration, while the variability in the depth and magnitude of subsurface enrichment reflects mixing and advection of water masses with different Ni inventories and biogeochemical histories. This interpretation is consistent with the broader West Atlantic, where Ni distributions are strongly governed by water-mass mixing, with remineralization providing an additional contribution (Stramma and England, 1999; Middag et al., 2020).

The relatively similar offshore dNi concentrations despite strongly contrasting river discharge therefore indicate that the offshore reactive Ni inventory is not directly proportional to instantaneous freshwater input. Instead, riverine Ni appears to be rapidly transformed and diluted within the estuarine–plume system, while its subsequent distribution is governed increasingly by biological cycling and redistribution among coastal and oceanic water masses. The elevated dNi concentrations in mangrove porewaters further demonstrate that mangroves can represent locally important Ni sources, although their signal is rapidly attenuated towards the coastal ocean. More broadly, these results demonstrate that riverine contributions to the coastal Ni cycle cannot be inferred from freshwater discharge alone, but depend on the extent of estuarine transformation, plume dynamics, biological cycling, and subsequent redistribution within the coastal and oceanic water-mass system.

CRediT authorship contribution statement

Cristian H. Krause: Writing – original draft. **Nico Fröhberg:** Data curation. **Leandro M. de Carvalho:** Supervision, Investigation, Funding acquisition. **Alexandre B. Schneider:** Investigation. **Kasley Barreto:** Methodology. **Andrea Koschinsky:** Project administration, Investigation.

Declaration of competing interest

The authors declare that they have no conflict of interest.

Acknowledgements

We thank Kechen Zhu, Albert Firus, Laurenz van Bonn and Gwendolyn Treguer for sample management in the clean laboratory, Elias Lilie for support with TMR sampling, Adrian Hollister and Caitlyn Kelly for sample mixing experiments, captain Rainer Hammacher and his crew of *RV Meteor* for excellent teamwork and equipment handling in the challenging and dynamic environment of the shallow Amazon estuary during research cruise M206. For the mangrove sampling campaign, we thank Sandra Pöhle for the excellent organization as well as sampling work and our partners at the University of Oldenburg and the Universidade Federal do Pará in Bragança for their advice, practical support and provision of laboratory facilities. The German Science Foundation (DFG) is acknowledged for funding *RV Meteor* cruise M206 (Amazon-GEOTRACES-2, reference number of the cruise proposal: GPF 20-1_057). The authors are also grateful to the financial support provided by FAURGS Foundation (Brazil, process 151164/2025), Deutscher Akademischer Austauschdienst (DAAD, project reference number 57705545) and CAPES (PROBRAL project AUXPE N° 88881.895128/2023-01).

Appendix A. Supplementary data

Supplementary data to this article can be found online at https://doi.org/10.1016/j.marchem.2026.104696.

Data availability

Data will be made available on request.

References

Achterberg, E.P., Braungardt, C., 1999. Stripping voltammetry for the determination of trace metal speciation and in-situ measurements of trace metal distributions in marine waters. Anal. Chim. Acta 400, 381–397. https://doi.org/10.1016/S0003-2670(99)00619-4.

Aguilar-Islas, A., Bridgestock, L., Bundy, R., Conway, T., Hayes, C., Heimbürger, L.-E., Planquette, H., Shaked, Y., 2024. Sampling and Sample-Handling Protocols for GEOTRACES Cruises.

Archer, C., Vance, D., Milne, A., Lohan, M.C., 2020. The oceanic biogeochemistry of nickel and its isotopes: new data from the South Atlantic and the Southern Ocean biogeochemical divide. EPSL 535, 116118. https://doi.org/10.1016/j.epsl.2020.116118.

Balistrieri, L.S., Murray, J.W., 1986. The surface chemistry of sediments from the Panama Basin: the influence of Mn oxides on metal adsorption. Geochim. Cosmochim. Acta 50, 2235–2243. https://doi.org/10.1016/0016-7037(86)90078-5.

Baxter, L.A.M., Bobrowski, A., Bond, A.M., Heath, G.A., Paul, R.L., Mrzljak, R., Zarebski, J., 1998. Electrochemical and spectroscopic investigation of the reduction of dimethylglyoxime at mercury electrodes in the presence of cobalt and nickel. Anal. Chem. 70, 1312–1323. https://doi.org/10.1021/ac9703616.

Bayen, S., 2012. Occurrence, bioavailability and toxic effects of trace metals and organic contaminants in mangrove ecosystems: a review. Environ. Int. 48, 84–101. https://doi.org/10.1016/j.envint.2012.07.008.

Bodin, N., N'Gom-Kâ, R., Kâ, S., Thiaw, O.T., Tito-de-Morais, L., Le Loc'h, F., Rozuel-Chartier, E., Auger, D., Chiffoleau, J.-F., 2013. Assessment of trace metal contamination in mangrove ecosystems from Senegal, West Africa. Chemosphere 90 (2), 150–157. https://doi.org/10.1016/j.chemosphere.2012.06.019.

Boyle, E.A., Huested, S.S., Grant, B., 1982. The chemical mass balance of the Amazon plume—II. Copper, nickel, and cadmium. Deep Sea Res. Part A Oceanogr. Res. Pap. 29, 1355–1364. https://doi.org/10.1016/0198-0149(82)90013-9.

Bruland, K.W., 1980. Oceanographic distributions of cadmium, zinc, nickel, and copper in the North Pacific. Earth Planet. Sci. Lett. 47, 176–198. https://doi.org/10.1016/0012-821X(80)90035-7.

Byrne, R.H., Kump, L.R., Cantrell, K.J., 1988. The influence of temperature and pH on trace metal speciation in seawater. Mar. Chem. 25, 163–181. https://doi.org/10.1016/0304-4203(88)90062-X.

Chakraborty, P., Ramteke, D., Chakraborty, S., 2015. Geochemical partitioning of Cu and Ni in mangrove sediments: relationships with their bioavailability. Mar. Pollut. Bull. 93, 194–201. https://doi.org/10.1016/j.marpolbul.2015.01.016.

Clough, B., 1998. Mangrove forest productivity and biomass accumulation in Hinchinbrook Channel, Australia. Mangroves Salt Marshes 2, 191–198. https://doi.org/10.1023/A:1009979610871.

Coleman, J.S., 1966. Chloride complexes of cobalt(II) in anion and cation exchangers. J. Inorg. Nucl. Chem. 28, 2371–2378. https://doi.org/10.1016/0022-1902(66)80128-8.

Costa de Souza, L., Carneiro dos Santos, C., Vasconcelos Júnior, N.T., Freitas Faial, K.C., Martins Corrêa, J.A., Alcântara Mendes, R., 2025. Trace metals in Amazonian rivers sediments from northern Brazil: spatial-temporal variations, sources, and ecological risks. Toxics 13 (10), 891. https://doi.org/10.3390/toxics13100891.

de Carvalho, L.M., Hollister, A.P., Trindade, C., Gledhill, M., Koschinsky, A., 2021. Distribution and size fractionation of nickel and cobalt species along the Amazon estuary and mixing plume. Mar. Chem. 236, 104019. https://doi.org/10.1016/j.marchem.2021.104019.

Dittmar, T., Hertkorn, N., Kattner, G., Lara, R.J., 2006. Mangroves, a major source of dissolved organic carbon to the oceans. Global Biogeochem. Cycles 20. https://doi.org/10.1029/2005GB002570.

Dittmar, T., Kattner, G., Lara, R.J., 2001. River or mangrove? Tracing major organic matter sources in tropical Brazilian coastal waters. Mar. Chem. 73, 253–271. https://doi.org/10.1016/S0304-4203(00)00110-9.

Dittmar, T., Lara, R., 2001. Driving forces behind nutrient and organic matter dynamics in a mangrove tidal creek in North Brazil. Estuar. Coast. Shelf Sci. 52, 249–259. https://doi.org/10.1006/ecss.2000.0743.

Espinoza Villar, J.C., Guyot, J.L., Ronchail, J., Cochonneau, G., Filizola, N., Fraizy, P., Labat, D., de Oliveira, E., Ordoñez, J.J., Vauchel, P., 2009. Contrasting regional discharge evolutions in the Amazon basin (1974-2004). J. Hydrol. 375, 297–311. https://doi.org/10.1016/j.jhydrol.2009.03.004.

Gao, Y., Zhou, C., Gaulier, C., Bratkic, A., Galceran, J., Puy, J., Zhang, H., Leermakers, M., Baeyens, W., 2019. Labile trace metal concentration measurements in marine environments: from coastal to open ocean areas. Trends Chem. 116, 92–101. https://doi.org/10.1016/j.trac.2019.04.027.

Gaulier, C., Zhou, C., Gao, Y., Guo, W., Reichstädter, M., Ma, T., Baeyens, W., Billon, G., 2021. Investigation on trace metal speciation and distribution in the Scheldt estuary. Sci. Total Environ. 757, 143827. https://doi.org/10.1016/j.scitotenv.2020.143827.

Han, H., Pan, D., 2021. Voltammetric methods for speciation analysis of trace metals in natural waters. Trends Environ. Anal. Chem. 29, e00119. https://doi.org/10.1016/j.teac.2021.e00119.

Harbison, P., 1986. Mangrove muds—a sink and a source for trace metals. Mar. Pollut. Bull. 17, 246–250. https://doi.org/10.1016/0025-326X(86)90057-3.

Hawco, N.J., Lam, P.J., Lee, J.-M., Ohnemus, D.C., Noble, A.E., Wyatt, N.J., Lohan, M.C., Saito, M.A., 2018. Cobalt scavenging in the mesopelagic ocean and its influence on global mass balance: synthesizing water column and sedimentary fluxes. Mar. Chem. 201, 151–166. https://doi.org/10.1016/j.marchem.2017.09.001.

Hollister, A.P., Kerr, M., Malki, K., Muhlbach, E., Robert, M., Tilney, C.L., Breitbart, M., Hubbard, K.A., Buck, K.N., 2020. Regeneration of macronutrients and trace metals during phytoplankton decay: an experimental study. Limnol. Oceanogr. 65, 1936–1960. https://doi.org/10.1002/lno.11429.

Hollister, A.P., Leon, M., Scholten, J., Van Beek, P., Gledhill, M., Koschinsky, A., 2022. Distribution and flux of trace metals (Al, Mn, Fe, Co, Ni, Cu, Zn, Cd, Pb and U) in the Amazon and Pará River estuary and mixing plume. ESS Open Arch. https://doi.org/10.1002/essoar.10512637.1.

Hollister, A.P., Whitby, H., Seidel, M., Lodeiro, P., Gledhill, M., Koschinsky, A., 2021. Dissolved concentrations and organic speciation of copper in the Amazon River estuary and mixing plume. Mar. Chem. 234, 104005. https://doi.org/10.1016/j.marchem.2021.104005.

John, S.G., Kelly, R.L., Bian, X., Fu, F., Smith, M.I., Lanning, N.T., Liang, H., Pasquier, B., Seelen, E.A., Holzer, M., Wasylenki, L., Conway, T.M., Fitzsimmons, J.N., Hutchins, D.A., Yang, S.-C., 2022. The biogeochemical balance of oceanic nickel cycling. Nat. Geosci. 15, 906–912. https://doi.org/10.1038/s41561-022-01045-7.

John, S.G., Liang, H., Pasquier, B., Holzer, M., Silva, S., 2024. Biogeochemical fluxes of nickel in the global oceans inferred from a diagnostic model. Global Biogeochem. Cycles 38, e2023GB008018. https://doi.org/10.1029/2023GB008018.

Koschinsky, A., Frank, M., de Carvalho, L., Firus, A., Freitas de Souza, M., Fröhberg, N., Haude, S., Hollister, A., Kaiser, D., Kalfouni, R., Kelly, C., Krause, C., Maguire, T.C., Moje, A., Lacerda, D., Lilie, E., Lima Reis Delatorre, A., Rezende, C., Sander, N., Schneider, A., Schnohr, M., Seidel, M., Stelzner, M., Treguer, G., Vahrenkamp, S., van Bonn, L., Xu, A., Zhu, K., Zindorf, M., 2025. Interactions of trace metals, DOM, and particles in the Amazon estuary and plume as key processes for trace metal and DOM fluxes into the Atlantic during the low-discharge period, Cruise No. M206, 01.12.2024 - 30.12.2024, Fortaleza (Brazil) - Belém (Brazil). METEOR-Berichte M206, 1–64. https://doi.org/10.48433/cr_m206.

Lacerda, L.D., Ferreira, A.C., Borges, R., Ward, R., 2022a. Mangroves of Brazil. In: Mangroves: Biodiversity, Livelihoods and Conservation. Springer Nature Singapore, Singapore, pp. 521–563.

Lacerda, L.D., Martinelli, L.A., Rezende, C.E., Mozeto, A.A., Ovalle, A.R.C., Victorio, R.L., Silva, C.A.R., Nogueira, F.B., 1988. The fate of trace metals in suspended matter in a mangrove creek during a tidal cycle. Sci. Total Environ. 75, 169–180. https://doi.org/10.1016/0048-9697(88)90030-7.

Lacerda, L.D., Ward, R.D., Borges, R., Ferreira, A.C., 2022b. Mangrove trace metal biogeochemistry response to global climate change. Front. For. Glob. Chang. 5, 817992. https://doi.org/10.3389/ffgc.2022.817992.

Lentz, S.J., 1995. Seasonal variations in the horizontal structure of the Amazon Plume inferred from historical hydrographic data. J. Geophys. Res., Oceans 100, 2391–2400. https://doi.org/10.1029/94JC01847.

Ma, F., Jagner, D., Renman, L., 1997. Mechanism for the electrochemical stripping reduction of the nickel and cobalt dimethylglyoxime complexes. Anal. Chem. 69, 1782–1784. https://doi.org/10.1021/ac961023s.

Marchand, C., Fernandez, J.-M., Moreton, B., 2016. Trace metal geochemistry in mangrove sediments and their transfer to mangrove plants (New Caledonia). Sci. Total Environ. 562, 216–227. https://doi.org/10.1016/j.scitotenv.2016.03.206.

Marchand, C., Fernandez, J.-M., Moreton, B., Landi, L., Lallier-Vergès, E., Baltzer, F., 2012. The partitioning of transitional metals (Fe, Mn, Ni, Cr) in mangrove sediments downstream of a ferrallitized ultramafic watershed (New Caledonia). Chem. Geol. 300–301, 70–80. https://doi.org/10.1016/j.chemgeo.2012.01.018.

Martino, M., Turner, A., Nimmo, M., 2004. Distribution, speciation and particle-water interactions of nickel in the Mersey Estuary, UK. Mar. Chem. 88, 161–177. https://doi.org/10.1016/j.marchem.2004.03.007.

Matos, C.R.L., Berrêdo, J.F., Machado, W., Metzger, E., Sanders, C.J., Faial, K.C.F., Cohen, M.C.L., 2022. Seasonal changes in metal and nutrient fluxes across the sediment-water interface in tropical mangrove creeks in the Amazon region. Appl. Geochem. 138, 105217. https://doi.org/10.1016/j.apgeochem.2022.105217.

McGill, J.T., 1958. Map of coastal landforms of the world. Geogr. Rev. 48, 402. https://doi.org/10.2307/212259.

Medeiros, P.M., Seidel, M., Ward, N.D., Carpenter, E.J., Gomes, H.R., Niggemann, J., Krusche, A.V., Richey, J.E., Yager, P.L., Dittmar, T., 2015. Fate of the Amazon River dissolved organic matter in the tropical Atlantic Ocean. Global Biogeochem. Cycles 29, 677–690. https://doi.org/10.1002/2015GB005115.

Melfi, A.J., Trescases, J.-J., Carvalho, A., de Oliveira, S.M.B., Ribeiro Filho, E., Formoso, M.L.L., 1988. The lateritic ore deposits of Brazil. Sci. Geol. Bull. 41, 5–36.

Middag, R., de Baar, H.J.W., Bruland, K.W., van Heuven, S.M.A.C., 2020. The distribution of nickel in the West-Atlantic Ocean, its relationship with phosphate and a comparison to cadmium and zinc. Front. Mar. Sci. 7, 105. https://doi.org/10.3389/fmars.2020.00105.

Milne, A., Landing, W., Bizimis, M., Morton, P., 2010. Determination of Mn, Fe, Co, Ni, Cu, Zn, Cd and Pb in seawater using high resolution magnetic sector inductively coupled plasma mass spectrometry (HR-ICP-MS). Anal. Chim. Acta 665, 200–207. https://doi.org/10.1016/j.aca.2010.03.027.

Monticelli, D., Caprara, S., 2015. Voltammetric tools for trace element speciation in fresh waters: methodologies, outcomes and future perspectives. Environ. Chem. 12, 683–705. https://doi.org/10.1071/EN14233.

Morris, D.F.C., Reed, G.L., Short, E.L., Slater, D.N., Waters, D.N., 1965. Nickel (II) chloride complexes in aqueous solution. J. Inorg. Nucl. Chem. 27, 377–382. https://doi.org/10.1016/0022-1902(65)80355-4.

Mota, A.M., Pinheiro, J.P., Simões Gonçalves, M.L., 2012. Electrochemical methods for speciation of trace elements in marine waters. Dynamic aspects. J. Phys. Chem. A 116, 6433–6442. https://doi.org/10.1021/jp2124636.

Motekaitis, R., Martell, A.E., 1987. Speciation of metals in the oceans. I. Inorganic complexes in seawater, and influence of added chelating agents. Mar. Chem. 21, 101–116. https://doi.org/10.1016/0304-4203(87)90032-6.

Moulatlet, G.M., Yacelga, N., Rico, A., Mora, A., Hauser-Davis, R.A., Cabrera, M., Capparelli, M.V., 2023. A systematic review on metal contamination due to mining activities in the Amazon basin and associated environmental hazards. Chemosphere 339, 139700. https://doi.org/10.1016/j.chemosphere.2023.139700.

Nimmo, M., van den Berg, C.M.G., Brown, J., 1989. The chemical speciation of dissolved nickel, copper, vanadium and iron in Liverpool Bay, Irish Sea. Estuar. Coast. Shelf Sci. 29, 57–74. https://doi.org/10.1016/0272-7714(89)90073-5.

Oliveira, S.M.B., Trescases, J.-J., Melfi, A.J., 1992. Lateritic nickel deposits of Brazil. Miner. Deposita 27, 137–146. https://doi.org/10.1007/BF00197099.

Prestes, Y.O., Borba, T.A.C., Silva, A.C., Rollnic, M., 2020. A discharge stationary model for the Pará-Amazon estuarine system. J. Hydrol. Reg. Stud. 28 (2020), 100668. https://doi.org/10.1016/j.ejrh.2020.100668.

Sander, S., Koschinsky, A., 2000. Onboard-ship redox speciation of chromium in diffuse hydrothermal fluids from the North Fiji Basin. Mar. Chem. 71, 83–102. https://doi.org/10.1016/S0304-4203(00)00042-6.

Santos, T.T.L., Marins, R.V., Alves, L.P., 2023. Review on metal contamination in equatorial estuaries in the Brazilian Northeast. Front. Earth Sci. 11, 1142649. https://doi.org/10.3389/feart.2023.1142649.

Schneider, A.B., Koschinsky, A., Krause, C.H., Gledhill, M., de Carvalho, L.M., 2022. Dynamic behavior of dissolved and soluble titanium along the salinity gradients in the Pará and Amazon estuarine system and associated plume. Mar. Chem. 238. https://doi.org/10.1016/j.marchem.2021.104067.

Sclater, F., Boyle, E., Edmond, J., 1976. On the marine geochemistry of nickel. Earth Planet. Sci. Lett. 31, 119–128. https://doi.org/10.1016/0012-821X(76)90103-5.

Silva, C.A.R., Lacerda, L.D., Rezende, C.E., 1990. Metals reservoir in a red mangrove forest. Biotropica 22, 339–345. https://doi.org/10.2307/2388551.

Smoak, J., Krest, J., Swarzenski, P., 2005. Geochemistry of the Amazon Estuary. In: Handbook of Environmental Chemistry, Volume 5: Water Pollution, pp. 71–90. https://doi.org/10.1007/698_5_029.

Stramma, L., England, M., 1999. On the water masses and mean circulation of the South Atlantic Ocean. J. Geophys. Res. 104 (C9), 20863–20883. https://doi.org/10.1029/1999JC900139.

Tam, N.F.Y., 2006. Pollution studies on mangroves in Hong Kong and mainland China. In: Wolanski, E. (Ed.), The Environment in Asia Pacific Harbours. Springer Netherlands, Dordrecht, pp. 147–163. https://doi.org/10.1007/1-4020-3655-8_11.

Tani, Y., Ohashi, M., Miyata, N., Seyama, H., Iwahori, K., Soma, M., 2004. Sorption of Co (II), Ni (II), and Zn (II) on biogenic manganese oxides produced by a Mn-oxidizing fungus, strain KR21-2. J. Environ. Sci. Health A Toxic Hazard. Subst. Environ. Eng. 39, 2641–2660. https://doi.org/10.1081/ESE-200027021.

Turner, A., Nimmo, M., Thuresson, K.A., 1998. Speciation and sorptive behaviour of nickel in an organic-rich estuary (Beaulieu, UK). Mar. Chem. 63, 105–118. https://doi.org/10.1016/S0304-4203(98)00054-1.

Twining, B.S., Baines, S.B., Vogt, S., Nelson, D.M., 2012. Role of diatoms in nickel biogeochemistry in the ocean. Global Biogeochem. Cycles 26. https://doi.org/10.1029/2011GB004233.

van den Berg, C.M.G., Khan, S.H., Daly, P.J., Riley, J.P., Turner, D.R., 1991. An electrochemical study of Ni, Sb, Se, Sn, U and V in the estuary of the Tamar. Estuar. Coast. Shelf Sci. 33, 309–322. https://doi.org/10.1016/0272-7714(91)90059-K.

Xu, A., Hathorne, E., Seidel, M., Liu, T., Asp, N.E., Koschinsky, A., Dittmar, T., Frank, M., 2025. The Amazonian mangrove systems accumulate and release dissolved neodymium and hafnium to the oceans. Nat. Commun. Earth Environ. 6 (1), 13. https://doi.org/10.1038/s43247-024-01989-1.

Yan, Z., Sun, X., Xu, Y., Zhang, Q., Li, X., 2017. Accumulation and tolerance of mangroves to heavy metals: a review. Curr. Pollut. Rep. 3, 302–317. https://doi.org/10.1007/s40726-017-0066-4.

Zhang, Z.-W., Xu, X.-R., Sun, Y.-X., Yu, S., Chen, Y.-S., Peng, J.-X., 2014. Heavy metal and organic contaminants in mangrove ecosystems of China: a review. Environ. Sci. Pollut. Res. Int. 21, 11938–11950. https://doi.org/10.1007/s11356-014-3100-8.